#3925

The Flow Properties of Rooms With Small Ventilation Openings

A. D. Gosman
P. V. Nielsen
A. Restivo
J. H. Whitelaw

Imperial College of Science and Technology,
Department of Mechanical Engineering,
Fluids Section,
London SW7 2BX, England

Measured and calculated properties relevant to the flow in ventilated rooms are reported. The measurements were obtained by laser-Doppler anemometry in a small-scale model room with a single square inlet. The calculations made use of a numerical procedure which solves, in finite-difference form, the elliptic partial-differential equations for three components of velocity, the pressure, the turbulence energy and its dissipation rate. Calculated results are shown to be in close agreement with the present measurements and with other available experimental data. With this justification, the procedure is used to quantify the dependence of the velocity characteristics of different geometric arrangements. The results provide guide lines for the design of ventilation systems.

1 Introduction

In previous papers, Nielsen, Restivo, and Whitelaw [1, 2] reported calculations of flow properties of relevance to ventilation and obtained with a two-dimensional calculation procedure. The results were restricted to flows which were two-dimensional or near two-dimensional. The purpose of the present paper is to report calculations for three-dimensional arrangements and, as before, to demonstrate their quantitative value by comparison with corresponding measurements.

The practical relevance of the investigation relates to the ventilation of rooms which is often achieved by supplying fresh, temperature-controlled air through a small, rectangular opening close to a ceiling. The return opening is normally located close to the floor but has considerably less influence on the velocity distributions within the room. There is a need for a procedure which will allow the velocity, and ultimately the temperature distributions, to be determined as a function of room geometry, mass flow and geometrical arrangement of a ventilation supply and return. The results presented here demonstrate the extent to which this can be achieved by the numerical solution of appropriate differential equations.

The calculation procedure is an extension of that described by Nielsen, Restivo and Whitelaw to include the third velocity component. This extension is relatively straight forward but results in a need for many more grid nodes and, as a result of this and comparatively slow convergence, long computing times. As a consequence, efforts have been made to increase the rate of convergence of the iterative procedure and the methodology and results of this effort are described. In addition, an economy of grid nodes is achieved by incorporating wall-jet development assumptions where these can be supported by reliable data; this precludes the need for a large number of grid nodes to describe the flow in the immediate vicinity of the inlet opening.

Contributed by the Fluids Engineering Division for publication in the JOURNAL OF FLUIDS ENGINEERING. Manuscript received by the Fluids Engineering Division, July 12, 1979.

The discretized nature of the solution method together with the assumptions inherent in a two-equation turbulence model imply that the calculated results can only be approximate. As a consequence, it is necessary to test the procedure by comparison with experimental data. Previous experimental studies of three-dimensional flow have been reported, for example, by Blum [3], Hestad [4] , and Jackman [5, 6] and some of these data are referred to in the results section. Unfortunately, they do not provide sufficient details to allow accurate comparisons and, to meet this requirement, new measurements are reported here and were obtained with the same laser-Doppler arrangement described by Nielsen, Restivo, and Whitelaw.

The flow configuration, anemometer and measured results are described in the following section. Section 3 introduces the calculation procedure and presents details of its application to the present flows. Predicted and measured flows are compared and discussed in section 4 and summary conclusions are presented in a final section.

2 Flow, Configuration, Anemometer and Experimental Results

Values of the longitudinal component of mean velocity and the corresponding normal stress were measured with a laser-Doppler anemometer. The anemometer, air-seeding arrangement and signal-processing instrumentation are identical to those described by Nielsen, Restivo, and Whitelaw.

The flow was arranged in a model fabricated from perspex and schematically represented in Fig. 1. The height of the model room, H, was 89.3 mm and the other dimensions correspond to the nondimensional quantities

$$L/H = 3.0, \quad W/H = 1.0, \quad h/H = 0.1,$$
$$w/H = 0.1 \text{ and } t/H = 0.16.$$

The inlet plane was preceded by a straight channel of square section, 270 mm long, and resulted in the initial profiles displayed in Fig. 2. It is clear that the mean velocity profiles have thick boundary layers of size comparable to $h/2$

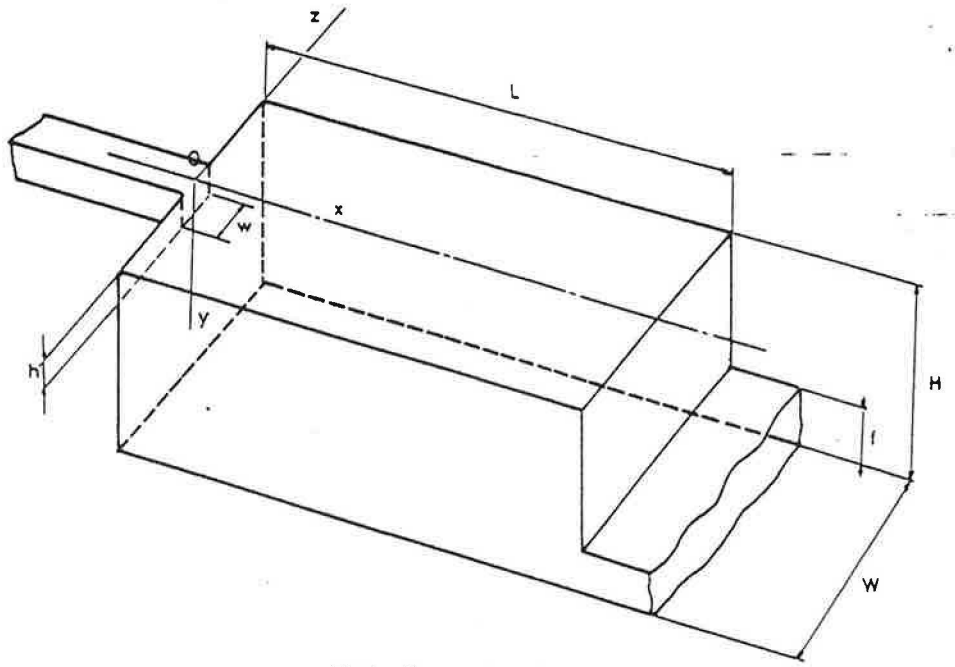

Fig. 1 Flow configuration

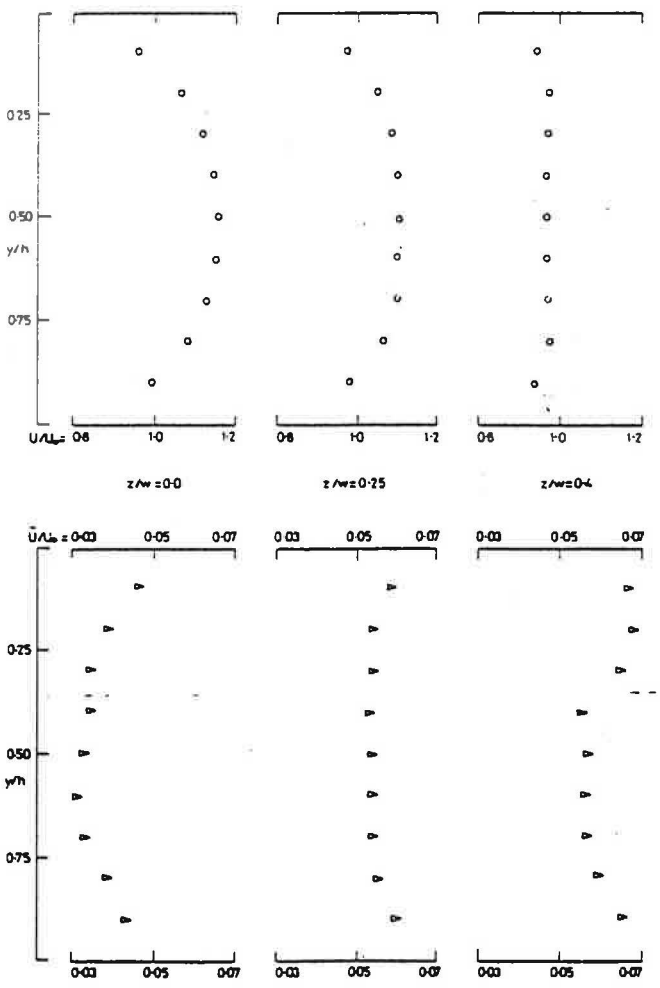

Fig. 2 Measured values of mean longitudinal velocity and the rms of the corresponding fluctuations in the inlet plane: $L/H=3$, $W/H=1$, $h/H=0.1$, $w/W=0.1$

although the centre line turbulence intensity does not exceed 3 percent. At the Reynolds number used for most of the experiments i.e. Re = 9000 based on h and the velocity at $h/2$, U_0, energy spectra were obtained in all regions of the flow and were typical of a turbulent flow; no influence of Reynolds number was detected in the present range of measurements.

Figure 3(a) presents profiles of longitudinal velocity at two different z-planes, corresponding to z/W values of 0.0 and 0.4, and Fig. 3(b) the maximum velocity decay in the symmetry plane of the jet. The calculations shown on these figures will be discussed in section 4. The measurements of Fig. 3(a) demonstrate that the square jet spreads in the y and z directions and, at x/H of 1.0, the maximum velocity in the symmetry plane is 20 times that at z/W of 0.4. Further downstream, at x/H of 2.0, the jet has spread to a more even velocity distribution but could not usefully be approximated by two-dimensional equations. As might be expected, the reverse flow velocities are less strongly influenced by the geometry of the inlet but are still significantly three-dimensional.

The upstream region of the inlet flow is represented, in greater detail, in Fig. 4. These measurements were obtained to allow comparisons with those of alternative inlet geometries and give further information on the development of a three dimensional wall jet issuing from a small orifice. The measurements are presented in non-dimensional form, with the maximum velocity U_m and the thickness at $U_m/2$ as normalising factors, and the results nearly reduce to a single curve, although some scatter is apparent. Rajaratnam and Pani [7] suggested that the velocity profiles are well described by a single nondimensional curve for x/h above 10, but the relative importance of h/H in this particular geometry is likely to have affected the jet development. The velocity decay in the jet under the ceiling is also compared with the square wall-jet results of Sforza and Herbst [8] and Rajaratnam and Pani [7] in Fig. 3(b), and the agreement is satisfactory up to x/H of about 2.5, until the jet decelerates towards the end wall.

Measured values of normal stress are not presented here because they are similar to those of the previous near two-dimensional results and carry little additional information.

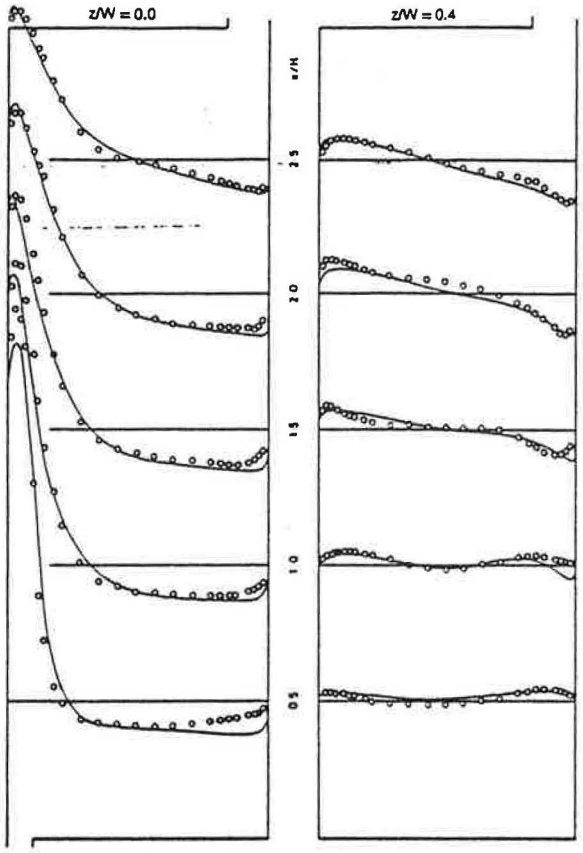

Fig. 3(a) Measured and calculated profiles of longitudinal velocity at z/W of 0.0 and 0.4

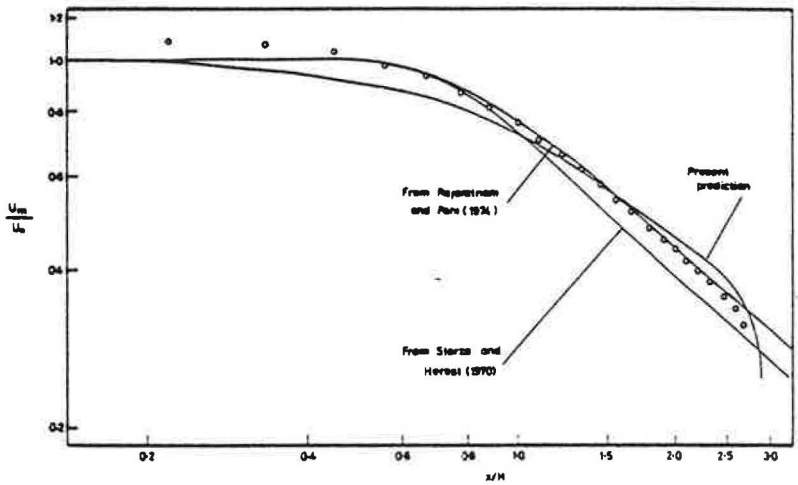

Fig. 3(b) Measured and calculated profiles of maximum velocity decay at z/W of 0.0
L/H = 3, W/H = 1, h/H = 0.1, w/H = 0.1.

The corresponding signals as examined on an oscilloscope and on power spectra did not exhibit predominant frequencies and the rms values varied from 0.25 U_0 in the exterior shear layer of the jet, at $z = 0$, $x = 0.5$H to $0.03U_0$ in the regions of lower mean velocity near the bottom corners below the inlet opening. The experimental uncertainty, previously discussed in reference [1], was better than ± 0.5 percent in mean velocity and ± 1 percent in rms values, for velocities above 0.5 m/s.

3 Calculation Procedure

The predictions were obtained by numerical solution of the time-averaged Navier-Stokes equations, supplement two-equation '$k-\epsilon$' turbulence model from which bulent Reynolds stresses are extracted. The equatio are of the general form

$$\frac{\partial}{\partial x_j}(\rho U_j \phi) = \frac{\partial}{\partial x_j}\left(\Gamma_\phi \frac{\partial \phi}{\partial x_j}\right) + S_\phi$$

where the dependent variable ϕ may be any of the f the three components of velocity U_1, U_2, U_3 referred to for convenience as U, V, and W resp turbulence energy k, and its dissipation rate ϵ. Defi the coefficients Γ_ϕ and S_ϕ corresponding to each of

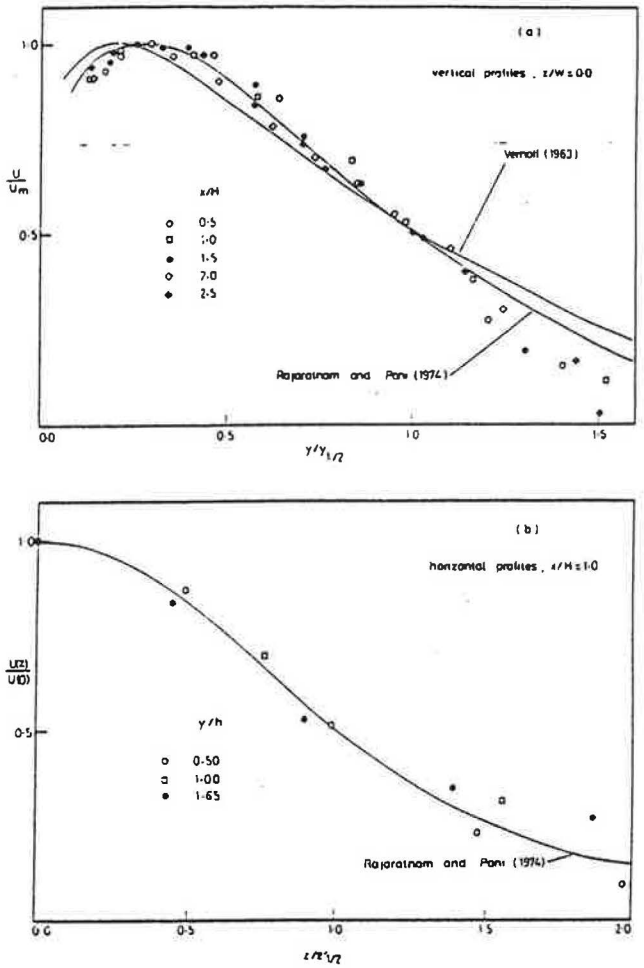

Fig. 4 Measured values of mean longitudinal velocity in the upstream region

listed in Table 1, as are the values of the empirical coefficients appearing in the turbulence model.

Table 1 Definition of Γ_ϕ and S_ϕ for conservation equations solved

Equation	ϕ	Γ_ϕ	S_ϕ
Continuity	1	0	0
Direction-i momentum	U_i	μ_{eff}	$-\frac{\partial P}{\partial x_i}+\frac{\partial}{\partial x_j}\left[\mu_{eff}\left(\frac{\partial U_i}{\partial x_j}+\frac{\partial U_j}{\partial x_i}\right)\right]$
Turbulence energy	k	μ_{eff}/σ_k	$G-\rho\epsilon$
Turbulence dissipation	ϵ	$\mu_{eff}/\sigma_\epsilon$	$\frac{\epsilon}{k}(C_1 G - C_2\rho\epsilon)$

Notes:

1. $G = \mu_{eff}\frac{\partial U_i}{\partial x_j}\left(\frac{\partial U_i}{\partial x_j}+\frac{\partial U_j}{\partial x_i}\right)$; $\mu_{eff} = \mu + \mu_t = \mu + C_\mu \rho k^2/\epsilon$
2. Turbulence model parameters assigned following values: $C_\mu = 0.09$, $C = 1.44$, $C_2 = 1.92$, $\sigma_k = 1$, $\sigma_\epsilon = 1.22$, $\kappa = 0.42$, $E = 9.79$.

Following now conventional practice, the boundary conditions at solid surfaces are applied indirectly via "wall functions" of the form:

$$V_R^+ = \frac{1}{\kappa}\ln(En^+) \tag{2}$$

$$\partial k/\partial n = 0 \tag{3}$$

$$\epsilon = C_\mu^{\frac{3}{4}} k^{\frac{3}{2}}/\kappa n \tag{4}$$

where $V_R^+ \equiv C_\mu^{\frac{1}{4}}\rho k^{\frac{1}{2}} V_R/\tau_w$, $n^+ \equiv C_\mu^{\frac{1}{4}}\rho k^{\frac{1}{2}} n/\mu$,

and n, V_R and τ_w are, respectively, the normal distance from, resultant velocity in planes parallel to, and resultant shear stress at, the wall. Values of the constants E and κ are given in Table 1.

For some of the calculations, the inlet conditions were also applied in an indirect manner as will be described below, while at the outlet the only prescription required was on the normal velocity, which was taken as uniform.

The differential equations were cast in finite-difference form and solved by a procedure akin to that employed by Nielsen, et al. [1, 2] in their calculations of two-dimensional flow, which in turn was based on the methodology described by Caretto, et al. [9] viz., use of staggered grids for the velocities, formulation of the difference equations in implicit, conservative form using hybrid central/upwind differencing (which insures realistic behavior in regions of both small and large mesh Reynolds number), recovery of pressure via a continuity-based equation and solution of the difference equations by an ADI-like iterative procedure.

The present procedure also shares with the earlier studies, and the three-dimensional furnace calculations of Abou Ellail et al. [10], the important feature of excluding the volume immediately surrounding the inlet from the normal calculations and instead imposing boundary conditions at its surface. This allows the more economical resolution of the jet-like flow emanating from the inlet, which is small in relation to the size of the room. The volume is prescribed large enough for the emerging jet to be adequately resolved by the numerical grid used elsewhere; the result is a significant reduction in the required computer storage and run time.

The downstream surface of the prescribed jet volume is important (the calculations proved to be relatively insensitive to the conditions imposed at entrainment boundaries) and, in principle, the conditions there may be determined by theoretical means (using, for example, an economical forward-marching procedure to determine, in a separate calculation, the jet development from entrance) or from experiment. For example, as demonstrated by the measurements of Rajaratnam and Pani [7], the velocity distributions in jets resulting from circular, square or other nearly axisymmetrical openings of the same area, issuing along a plane surface are all well described by the same nondimensional mean profiles at locations downstream of around 10 diameters. The decay of the maximum velocity and the growth rates were also shown to be similar. In view of these findings, available wall jet data has been used as a basis for the prescription of the new boundary conditions required in cases where measured data is not available and the relative dimension h/H is small enough for the jet to develop before the influence of the walls of the room becomes important. Where this data does not include turbulence measurements, the required parameters are estimated by solving the turbulence equations with the measured velocities inserted. The particular treatments employed in the present calculations will be described as each case is presented.

The rate of convergence of the iterative method is crucial to three-dimensional procedures of the present kind and special steps were taken to accelerate it, while keeping storage requirements within reasonable bounds. Thus, with one exception, the ADI solution technique was confined to a single set of cross-sectional planes in order to limit the coefficient storage requirements, while improved account was taken of plane-to-plane interactions using block velocity and

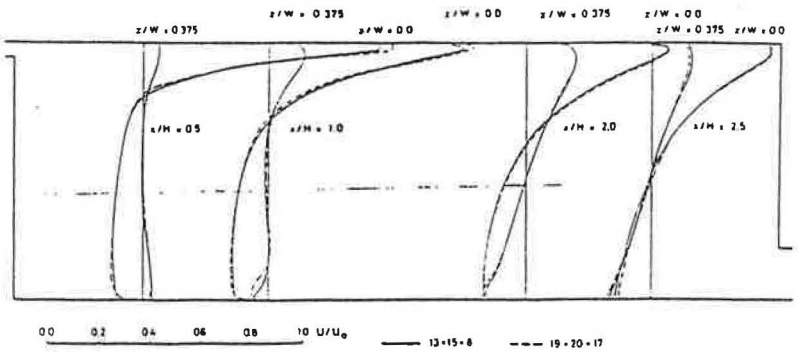

Fig. 5 Influence of number of grid nodes on calculated values of mean longitudinal velocity: $L/H=3$, $W/H=1$, $h/H=0.056$, $w/W=0.5$

pressure adjustments based on global continuity and momentum conservation. The sole exception was the pressure equations, whose strongly elliptic character favoured the use of a full three-dimensional ADI procedure, and whose particular coefficient structure allowed this to be done using little additional storage. These techniques reduced computing times by some 50% of those for the unmodified procedure.

4 Calculated Results

The influence of the number of grid nodes on the solutions obtained was investigated and typical results are shown in Fig. 5 for conditions corresponding to the second entry of Table 2. These results, which were obtained without the special inlet treatment described earlier, show discrepancies of the order of 5 percent of the maximum velocity between a numerical grid with $13\times15\times8$ and $19\times20\times17$ nodes. Tests with smaller numbers of nodes indicated a monotonic convergence of the results towards those with the maximum number of nodes. It is clear that discrepancies as indicated by Fig. 5 will be associated with all practical numbers of grid nodes but, as the comparison of the following paragraphs will show, this order of precision is adequate for ventilation design purposes, and the associated computing time, on a CDC 6600, of about 17 min for a $13\times15\times8$ grids (corresponding to 210 iterations and residual mass sources less than 1 percent of the through flow) may also be regarded as acceptable.

To establish confidence in the overall procedure and to attempt to quantify precision by comparing calculations with measurements, three geometrical configurations were considered and are indicated in Table 2.

Table 2 Configurations used for comparisons of Figs. 3, 6, and 7

Source of experimental data	L/H	W/H	h/H	w/H	Re
Present measurements	3.0	1.0	0.1	0.1	9,000
Nielson, Restivo, and Whitelaw [1]	3.0	1.0	0.056	0.5	5,000
Blum [3]	3.0	1.0	circular diffuser $d/H=0.04$		93,000

The general features of these flows are indicated by the predicted vector plots[1] of Fig. 6(*a*), which relate to the geometry of reference [1]. The circulation patterns are clearly different in the elevations at $z=0$ and $z=0.47\ W$, with the centre of the circulation vortex located further upstream close to the side wall and opposite flow directions in the bottom area below the opening. Inspection of the plan view at $y=0.97H$ indicates two vortices in this area rotating about near-vertical axes. These calculations were performed with a $13\times15\times8$ grid and measured downstream boundary ditions as described below.

The velocity profiles of Figs. 6(*b*) and 6(*c*) to relate to same geometry and indicate differences bet measurements and calculations of up to 10 percent of maximum velocity, which occur mainly in the vicinity o side walls near the ceiling and in the regions of lower vel in the reverse flow. The maximum reverse flow velo measured close to the side walls, is predicted within 2 per of the maximum velocity. Figure 6(*c*) indicates that predicted and measured decay of the maximum velocity in jet downstream of the starting plane corresponds to the stage of development of a slender three-dimensional wall designated as the "characteristic decay region" by Sfc [11].

For these calculations, measured profiles of longitud velocity were prescribed at the grid nodes located in the pl of $x/H=1.0$ and y/H up to 0.12. The longitudinal velocit the remaining nodes, and the other variables at all nodes, w calculated over the entire flow domain. The results sho smooth variation of calculated properties at the nodes jacent to $x/H=1.0$ and $y/H<0.12$ as may be seen from F 6(*a*).

The present measurements are also adequately represen by the calculation procedure, as indicated by Fig. 3(*a*) and and the maximum discrepancy between calculation a measurement is of the order of 5 percent of the inlet veloci The results were obtained without the special inlet treatm which was unnecessary due to the comparatively large va of h/H. The grid had $14\times14\times9$ nodes and a constant veloc profile was prescribed at the inlet.

In the measurements of Blum [3], obtained with a Pit tube, the jet issued from a circular opening of diameter sm compared to other room dimensions. The results, which w obtained with a $13\times15\times8$ grid, are shown on Fig. 7 a indicate a discrepancy of around 10 percent in the horizon spreading rate of the jet adjacent to the ceiling and near to side walls at $x/H=2.14$. The decay of maximum velocity also slightly underpredicted, with an associated difference 5 percent in the centre-line at the $x/H=2.54$. The gene agreement is, however, satisfactory and in the reverse flo for example, the discrepancies are below 1 percent of maximum flow velocity. Due to the small inlet dimensio calculations with boundary conditions prescribed at the in opening lead to poor agreement with the measured data, w the present number of grid nodes, as shown in Fig. 7(*b*) a better results were obtained again with the special in treatment described in section 3. The longitudinal velocity w prescribed at the nodes in the volume limited by the planes $x=1.14H$, $y=0.1H$ and $z=0.31H$, and in these nodes velocity was assumed to conform with non-dimensio profiles typical of a developed wall jet, in line w Rajaratnam and Pani [7] and the turbulence parameters we

[1] These do not show the vectors in the outlet plane; however the flow there is prescribed as horizontal and uniform, as explained earlier.

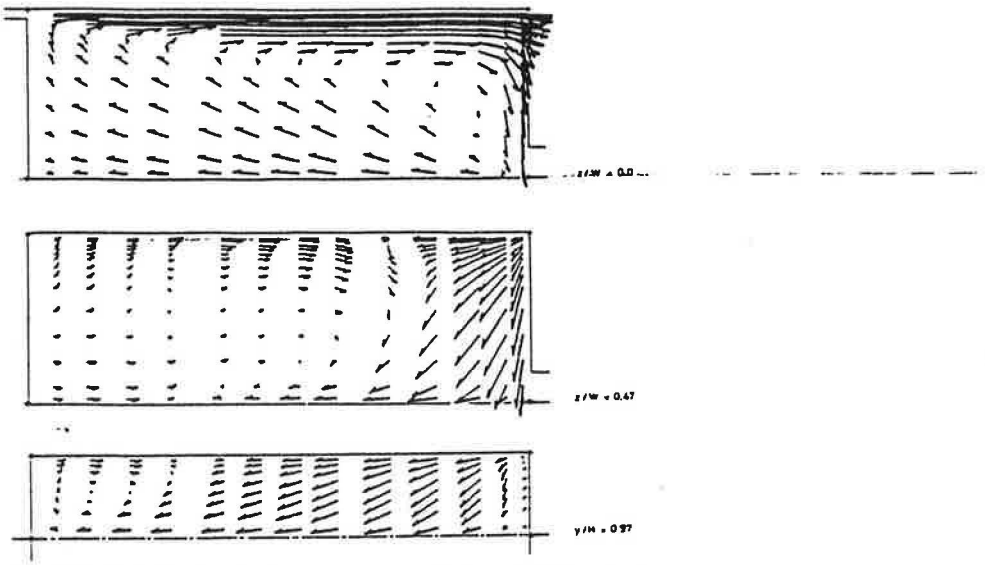

Fig. 6(a) Calculated velocity vectors at $z/W=0$ and 0.47 and at $y/H=0.97$

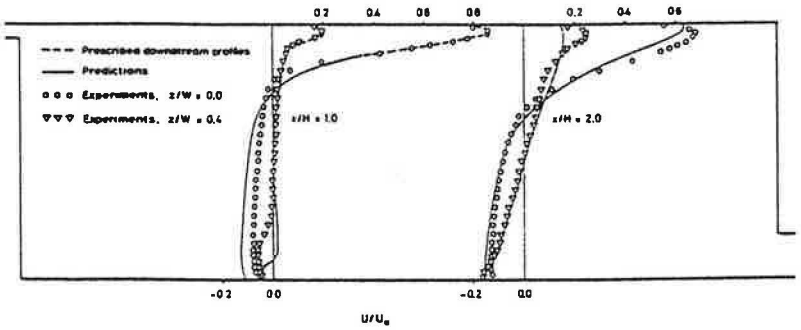

Fig. 6(b) Measured and calculated profiles of mean longitudinal velocity at $x/H=1$ and 2

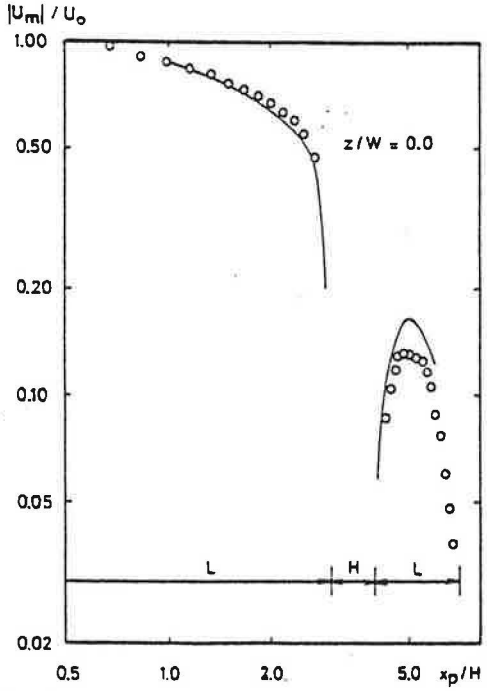

Fig. 6(c) Measured and calculated profiles of maximum velocity around the perimeter, x_p.
$L/H=3$, $W/H=1$, $h/H=0.056$, $w/W=0.5$.

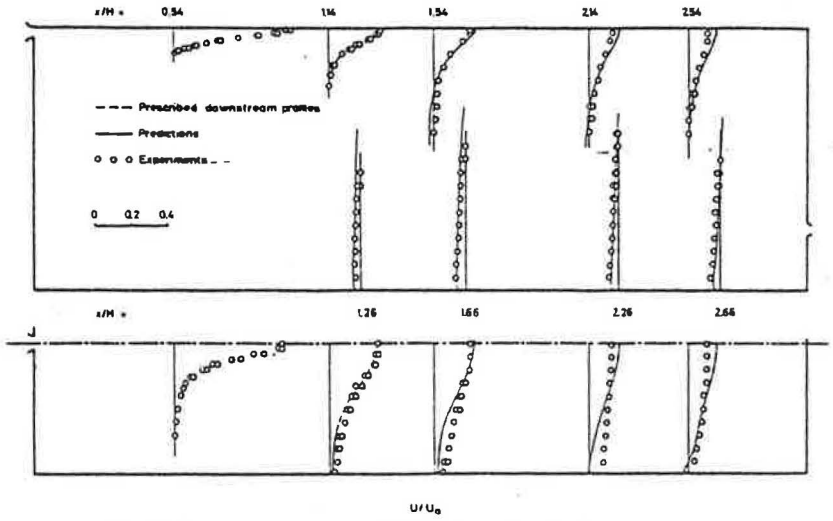

Fig. 7(a) Comparison of calculated mean longitudinal velocity with the measurements of Blum [3]

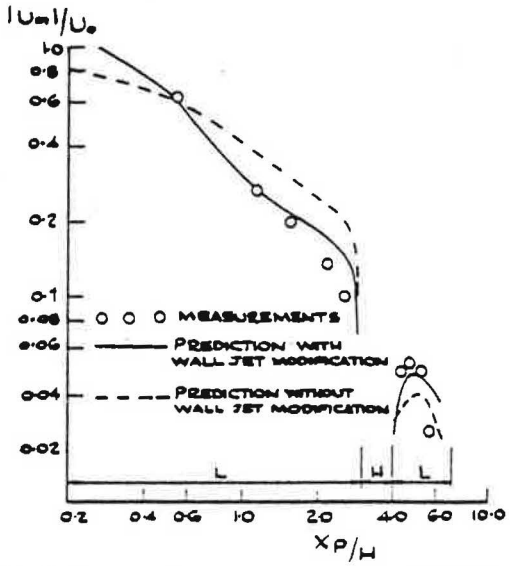

Fig. 7(b) Comparison of calculated maximum velocity around the perimeter with the measurements of Blum [3]. $L/H=3$, $W/H=1$, $d/H=0.04$.

estimated as described earlier. The longitudinal velocity at the remaining nodes and the node values of all other properties were calculated by the numerical procedure: it should be noted that the remaining volume and number of nodes were both large in relation to the prescribed region, so in no sense is this practice equivalent to prescribing the entire flow field.

5 Discussion

In general, the results described in the previous section confirm that the calculation procedure is capable of representing the experimentally determined flow patterns with a typical precision of 5% of the maximum velocity. To achieve this order of precision requires more than 1500 nodes to represent a symmetrical half of the flow and the use of an inlet jet-flow correlation for small inlet area. Discrepancies increase as the number of nodes is decreased and as one or both dimensions of the air supply arrangement is decreased. Attempts to perform calculations with a similar number of nodes and without the initial-jet-flow correlations resulted in significantly greater discrepancies as indicated in Fig. 7(*b*). This clearly demonstrates the difficulty associated with the numerical calculations of all flows where small changes in dimensions can lead to large effects.

Since the present calculations involve a significant use of computer time, with associated cost, it is appropriate to consider the possibility that a simpler turbulence model might adequately represent the present flow. Figure 8 presents calculated contours of turbulent kinetic energy and dissipation length scale ($l=k^{3/2}/\epsilon$) associated with the geometry of Blum, and shows the variations of both properties. The variations in length scale, in particular, are fairly regular and an algebraic formulation may be possible. In view of the range of geometric arrangements associated with ventilation, the greater generality associated with the transport model renders it more appropriate.

The capabilities of the present procedure and its precision have been established in the previous paragraphs and, on this basis, the results of Fig. 9 were obtained to provide new information of relevance to designers. They relate to a square inlet, a room of square cross section ($W/H=1$) and a length to height ratio of 3.0, and were obtained with prescribed inlet conditions similar to those used to predict Blum's measured

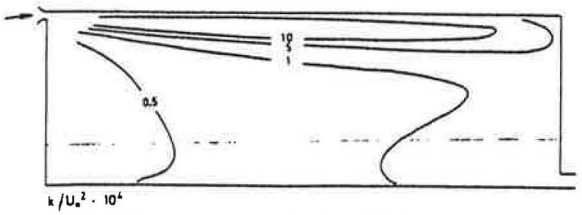

Fig. 8(a) Contours of turbulence kinetic energy

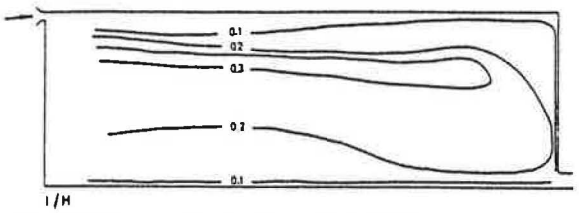

Fig. 8(b) Contours of the length scale $l = k^{3/2}/\epsilon$ $L/H = 3$, $W/H = 1$, $d/H = 0.04$

data. The maximum velocity in the reverse flow, U_{rm}, is plotted against the relative area of the inlet, a/A $(= hw/(HW))$: it is clear that increasing the size of the supply opening also increases the maximum reverse velocity, if the inlet velocity U_0 is kept constant. Closer examination of Fig. 9 indicates that, for small openings, U_{rm}/U_0 tends to vary as $(a/A)^{0.5}$, i.e. the maximum reverse velocity is approximately proportional to the square root of the momentum flow rate at the inlet opening $\sqrt{a}U_0$. This is in accord with the findings of reference 5 for rooms with side wall mounted diffusers.

In practice, the flow rate is commonly determined by air refreshment requirements, i.e. aU_0 must be assumed constant; then U_{rm} increases with decreasing a, and tends to vary as $a^{-0.5}$ for small a/A ratios. In Fig. 9 the results from the earlier two-dimensional calculations have been included and it is clear that although U_{rm} tends to vary as $a^{-0.5}$ in both cases for constant mass flow rate, the two-dimensional values are higher (10 percent at $a/A = 0.003$ and 30 percent at $a/A = 0.01$).

5 Conclusions

The following more important conclusions may be extracted from the previous text:

1. The measurements provide further evidence of the flow patterns associated with small inlet openings and in particular of the extent of three-dimensionality in the inlet region and in the occupied area of rooms. For identical inlet velocity, the velocity levels associated with the square opening were lower than those for the half width slot of reference [1], as was expected in view of the different inlet areas, but the overall flow patterns in both geometries are closely related.

2. The present numerical solutions of the three-dimensional flow equations allow the representation of available measurements with a precision of around 5 percent of the maximum velocity. The inclusion of differential equations for the conservation of turbulent kinetic energy and dissipation rate is desirable but may not be necessary. The numerical precision is limited by the number of nodes which can be afforded; the precision quoted relates to approximately 1500 nodes in a symmetrical half plane and with a special inlet treatment to obviate the need for a concentration of nodes in this region.

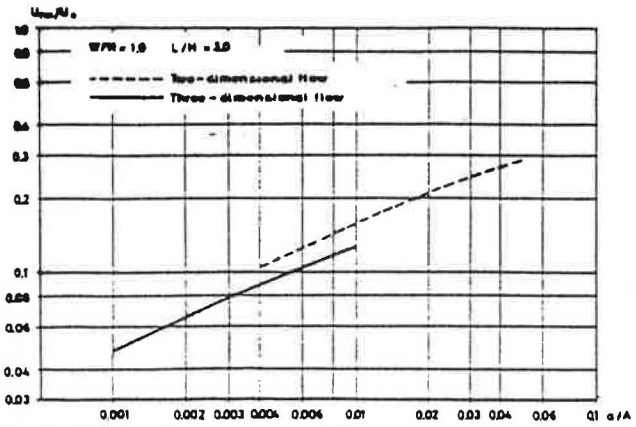

Fig. 9 Calculated nondimensional, maximum reverse velocity as a function of relative inlet area

3. The results indicate that the maximum velocity in the reverse flow is essentially determined by the area of the supply opening and not by its shape, provided the overall dimensions of the opening are small and they also show that U_{rm}/U_0 tends to vary as $(a/A)^{0.5}$ which is consistent with the earlier two-dimensional conclusions although the present values are some 10 to 30 percent lower.

Acknowledgments

The authors wish to acknowledge personal financial support from the Danish Government Fund for Scientific and Industrial Research (PVN) and from Comissão Permanente INVOTAN and Instituto Nacional de Investigacao Cientifica (AR). Danfoss A/S (PVN) and the University of Oporto (AR) kindly released their staff to allow this work to be carried out. The experimental and computational work was supported by the Science Research Council and part of the calculations by Danfoss A/S, to whom all authors record their thanks.

References

1 Nielsen, P. V., Restivo, A., and Whitelaw, J. H., "The Velocity Characteristics of Ventilated Rooms, ASME JOURNAL FLUIDS ENGINEERING, Vol. 100, 1968, p. 308.

2 Nielsen, P. V., Restivo, A. and Whitelaw, J. H., "Buoyancy Affected Flows in Ventilated Rooms," To be published in *Numerical Heat Transfer Journal.*

3 Blum, W., 1956, Diplomarbeit, T. H. Aachen.

4 Hestad, T., "En dimensjoneringsmetode for tilluftsorganer basert på teori, fullskalaforsøk og praktisk erfaring," Tekniska meddelanden nr. 83, Inst. för Uppvärmnings-och Ventilationsteknik, KTH, Stockholm, 1975.

5 Jackman, P. J., "Air Movement in Rooms With Side-Wall Mounted Grilles - a Design Procedure," HVRA, Report No. 65, 1970.

6 Jackman, P. J., "Air Movement in Rooms With Sill-Mounted Grilles - a Design Procedure," HVRA, Report No. 71, 1971.

7 Rajaratnam, N., and Pani, B. S., "Three-Dimensional Turbulent Wall Jets," *Proc. A.S.C.E.*, J. Hydraul. Div., Vol. 100, 1974, p. 69.

8 Sforza, P. M. and Herbst, G., 1970. A study of three-dimensional incompressible turbulent wall jets, J. AIAA, 8, 276.

9 Caretto, L. S., Gosman, A. D., Patankar, S. V., and Spalding, D. B., "Two Calculation Procedures for Steady, Three-Dimensional Flows With Recirculation," *Proc. 3rd Int. Conference on Num. Methods in Fluid Dynamics*, Springer Verlag, 1972.

10 Abou Ellail, M. M. M., Gosman, A. D., Lockwood, F. C. and Megahed, I. E. A., "The Prediction of Reaction and Heat Transfer in Three-Dimensional Combustion Chambers," Presented at AIAA/ASME Thermophysics and Heat Transfer Conference, Palo Alto, May 1978.

11 Sforza, P. M., "Three-Dimensional Free Jets and Wall Jets: Applications to Heating and Ventilation," Polytechnic Institute of New York, 1977.